The Martian Slope Winds and the Nocturnal PBL Jet

HANNU SAVIJÄRVI

Department of Meteorology, University of Helsinki, Helsinki, Finland

TERO SIILI

Finnish Meteorological Institute, Helsinki, Finland

(Manuscript received 18 October 1991, in final form 10 March 1992)

ABSTRACT

The summertime Martian PBL diurnal wind variation, slope winds, and the nocturnal low-level jets were studied using Prandtl's theory, a mesoscale numerical model, and *Viking* lander observations. During moderate prevailing large-scale flow, nocturnal jets were simulated that were rather similar to those on Earth. They were mainly caused by inertial oscillation after sunset with some contribution from the slope wind effects over sloping regions (which are very common in Mars). During weak large-scale flow, shallow nocturnal drainage flows with strong vertical shear developed over the cold Martian slopes. At middle and high latitudes, these katabatic winds tended to turn to flow along the slope by dawn (due to the Coriolis force). For sufficiently steep slopes, near-surface drainage winds could reach considerable speeds. In contrast, the typical afternoon upslope winds were vertically homogeneous up to 2–3 km and weak (only 1–3 m s^{-1} in magnitude), even over relatively steep large-scale slopes.

1. Introduction

Drainage or katabatic winds form when nocturnally cooled negatively buoyant dense air is accelerated down cold slopes by gravity. Daytime anabatic winds are likewise accelerated upslope by positive buoyancy over sun-heated warm slopes. Even gentle slopes of 1:1000 can create drainage winds of 1–2 m s^{-1} on Earth (Stull 1988). Favorable conditions for these diurnal mesoscale winds include terrain sloping over a large area, strong diurnal surface temperature variation, and weak ambient winds. These conditions are typical on Mars in summer. Large-scale sloping plains are common on Mars, where there are no oceans, but the elevation differences of the desertlike surface are as large as 25 km (e.g., Pollack et al. 1981). The *Viking* landers (VL) observed weak ambient winds in summertime, and diurnal temperature variation amplitudes were about three times those of Earth deserts (Hess et al. 1977; Leovy 1982). Therefore, one might expect slope winds to be a common and regular feature of local Martian weather and climate in the summer, while in the autumn, winter, and spring, the prevailing strong westerlies, frequent baroclinic disturbances, and dust storms may mask the weaker local slope winds. Indeed, the *Viking* landers, which set down on large-scale slopes of about 1:600, reported regular summertime diurnal surface wind hodographs with clockwise rotation at VL-2 and counterclockwise rotation at VL-1. These have received little attention, however, since the initial discussion of the possible influences of tidal and slope effects on them (Hess et al. 1977; Leovy 1982).

Blumsack et al. (1973) made an initial pre-*Viking* study of the Martian slope winds. More recently, Ye et al. (1990) made a thorough study of the Martian daytime upslope flow using both analytical approaches and a 2D mesoscale numerical model (which assumed dust-free and dry conditions), but they did not compare their results with the VL data and they did not extend their published analysis to the nocturnal drainage flow. In this article, the 2D version of the University of Helsinki Mesoscale Model is applied to the slope winds on Mars, as in Ye et al. (1990). The full diurnal cycle is simulated, the model includes dust and moisture, and the results are compared with the VL observations. We also study the interaction of the drainage flow with the nocturnal low-level jet on Mars, which may occur if there is a background flow.

The radiation schemes for our model were developed and validated in Savijärvi (1991b) for dustless conditions. The dust scheme and summertime simulations for a flat Mars with the 1D model version were described in Savijärvi (1991c) (S1D), concentrating, in S1D, on the thermodynamics of the Martian boundary layer, that is, the temperature profile and its diurnal variation as the response to the strong radiative and turbulent heating and cooling in the thin dusty CO_2

Corresponding author address: Dr. H. I. Savijärvi, Department of Meteorology, University of Helsinki, Hallituskatu 11, SF-00100 Helsinki, Finland.

TABLE 1. Key variables in the basic simulations described in the text.

Site	VL-1	VL-2	Bosporos Planum	Arsia Mons
Latitude (°N)	22.5	48	−45	−15
T (K)[a]	225	225	220	213
p (mb)[a]	7.65	7.65	7.0	5.0
v_g (m s^{-1})	10	0	0	0
Slope angle (deg)	0.10	0.10	0.15	0.27
Areocentric longitude (L_s)[b] (deg)	100	115	310	310

[a] Initial values in the lowest point of the calculation area.
[b] L_s is seasonal index ($L_s = 0°$ at northern spring equinox, $L_s = 90°$ at northern summer solstice).

atmosphere. The 1D model simulated the observed VL-1 and VL-2 temperature entry profiles and the diurnal surface temperature cycle quite well. Another companion investigation of the U.S. Great Plains slope winds and the strong NLLJ has been made recently (Savijärvi 1991a). An interesting comparison of the Great Plains simulations with the present VL-1 site simulations can be made here, since, by lucky coincidence, the external conditions [latitude belt, time of year, length of day (86 400 s vs 88 775 s = sol), terrain slope angle, direction and roughness, and even the ambient wind speed and direction] happen to be rather similar in the two cases.

The VL landing conditions were quite successfully predicted by the first Martian general circulation model (Pollack et al. 1976; Pollack 1991). We will follow here the tradition of bold weather forecasts for Mars by finally presenting a prediction of the expected summertime wind and temperature diurnal cycles for the proposed weather station sites of the European Space Agency (ESA) MARSNET mission (Chicarro et al. 1991). The results may also help in the systems design of future mission instrumentations.

2. The model and the simulations

The 2D version of the University of Helsinki Mesoscale Model is a σ-coordinate hydrostatic primitive equations model. It is like a slice (a $x\sigma$-cross section) of an ordinary weather forecast or general circulation model but with fine horizontal and vertical resolution. It has been used to simulate many surface-driven mesoscale phenomena of Earth's lower atmosphere, such as coastal convergence and topographic lifting (Alestalo and Savijärvi 1985), sea breezes (Neumann and Savijärvi 1986; Savijärvi and Alestalo 1988), urban heat islands (Savijärvi 1985), effective roughness of coastal regions (Vihma and Savijärvi 1991), diurnal cycles, slope winds, and nocturnal jets (Savijärvi 1991a). The model, originally that of Alpert et al. (1982), thus seems to be well tested for Earth. Here the parameters have been changed appropriate to those for Mars, more specifically for the *Viking* lander site conditions during the first few sols (days) of the landers on Mars. Table 1 lists key values for these and the MARSNET site simulations. In all experiments, the soil thermal inertia parameter is 220 W m^{-2} s$^{1/2}$ K^{-1}, z_0 = 1 cm, albedo = 0.2, initial lapse rate = 2 K km^{-1}, and dust optical depth τ = 0.4. The dust properties are based on Pollack (1982). A more complete description of the astronomic, atmospheric, and soil values is given in S1D where the 1D version and the subgrid-scale parameterizations were described in detail.

The model equations are in the references mentioned above. Briefly, advection is Lagrangian with cubic spline interpolation, mesoscale pressure gradient force is integrated with an Adams–Bashworth scheme, and horizontal diffusion is a weak low-pass filter. The vertical diffusion scheme, its boundary conditions, and the implicit numerical solution methods are similar to those used, for example, in the ECMWF weather forecast model, with a Monin–Obukhov surface-layer representation and stability- and wind-shear-dependent diffusion coefficients aloft (Louis 1979). The main difference is that we use observational Earth (the "Kansas experiment") nondimensional stability functions directly, as our model is intended to simulate local mesoscale flow over a supposedly homogeneous surface. The scheme was described and compared with the NSSL Oklahoma tower observations in Savijärvi (1991a). It was found to work well. The same scheme is used for Mars; some diffusion coefficients of the VL-1 site simulation are shown in Fig. 9. The results are sensitive to the surface-layer scheme, but fortunately the Monin–Obukhov similarity theory seems to be applicable on Mars (Sutton et al. 1978). Surface temperature is predicted in our model with the force–restore method (e.g., Dickinson 1988), which is based on the analytic solution of heat diffusion to the soil with cyclic forcing. Saturation is not considered, that is, the sky is clear except for dust, and the atmospheric moisture is assumed to be initially well mixed in the Martian PBL with total precipitable water contents of 17 μm [PWC of 15–20 μm is observed for the VL-1 latitude in summer (Haberle 1986)]. Soil moisture (wetness) was fixed to a value (0.07%), which preserved the PWC during the integrations. These rather uncertain moisture values have, fortunately, only a small impact to the dynamics (through radiation). The radiation schemes were carefully tested for Mars, having a narrowband model of CO_2 as a reference and also including the effects of dust on the shortwave and moisture on the longwave (Savijärvi 1991b, S1D). Since moisture and pressure vary only slowly on Mars during the day, in contrast with temperature, the CO_2 and H_2O longwave emissivities are updated only every sixth hour, while the remaining radiation calculations are done every time step using the actual rapidly changing temperatures and solar height angles.

The 1D version was quite successful in simulating the diurnal surface temperature cycles and the temperature profiles as observed by the *Viking* landers during and after their entry (S1D). Here the 2D model's horizontal gridlength is 30 km and the 11 levels are at the approximate heights of 1.6, 25, 60, 125, 250, 460, 850, 1500, 2800, 5000, and 7500 m above the Martian ground. A slope is set in the middle 600 km of the 2000-km wide simulation area, with 700-km level land on both sides. The slope angles and directions for the four sites are based on the large-scale topography of Pollack et al. (1981). The boundary conditions are vanishing horizontal gradients in the vertical boundaries, and $\dot{\sigma} = 0$ at the top and bottom. The integrations start at 0600 local lander time (LLT) at sol 1 with a short 20 s time step to eliminate nonlinear instabilities of diffusion. The results shown are for sol 2, whereafter the model repeats its daily cycle almost unchanged, being in an approximate radiative–convective climatological equilibrium as discussed in S1D. The long initialization guarantees realistic "initial" conditions for both the uphill and downhill circulations. As with the 1D version, the 2D model results are rather insensitive to the initial temperature profile and numerics (e.g., horizontal and vertical grid spacing and model top height).

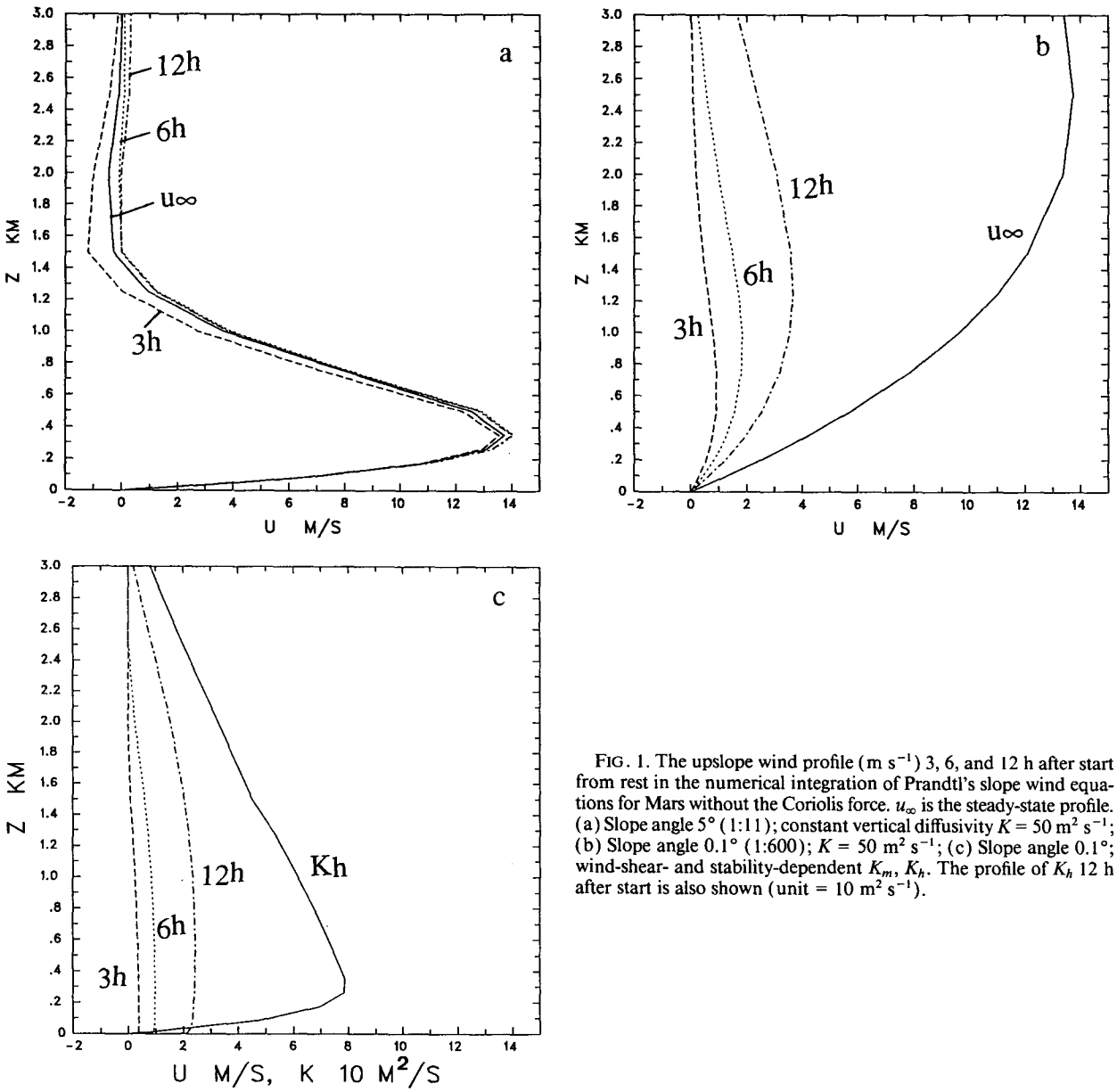

FIG. 1. The upslope wind profile (m s^{-1}) 3, 6, and 12 h after start from rest in the numerical integration of Prandtl's slope wind equations for Mars without the Coriolis force. u_∞ is the steady-state profile. (a) Slope angle 5° (1:11); constant vertical diffusivity $K = 50$ m^2 s^{-1}; (b) Slope angle 0.1° (1:600); $K = 50$ m^2 s^{-1}; (c) Slope angle 0.1°; wind-shear- and stability-dependent K_m, K_h. The profile of K_h 12 h after start is also shown (unit = 10 m^2 s^{-1}).

3. The Martian slope winds: Prandtl theory

The Martian daytime upslope wind mechanism was first studied by solving the linear Prandtl slope wind equations both analytically and numerically, as in Ye et al. (1990) and Savijärvi (1991a). Radiative heating was neglected on the basis that it is in the growing Martian mixed layer "only" about 40 K day^{-1}, while the turbulent heating is of the order of 100 K day^{-1} (S1D; Fig. 7; 1000 LLT). Also the Coriolis force was first neglected. Figure 1 shows the upslope wind component 3, 6, and 12 h after start from rest, when the slope is made 15 K warmer than undisturbed air at the same altitude. The background stability $\partial\bar{\theta}/\partial z$ is 2 K km^{-1}, $K = 50$ m^2 s^{-1}, and $g/\bar{\theta} = 3.71/230$ m s^{-2} K. The values are based on the VL data and the 1D model simulations and are supposed to be representative of the growing Martian mixed layer during a summer morning. The terrain slope is 5° (1:11) in Fig. 1a and 0.1° (1:570) in Fig. 1b. One can see the quick growth of the upslope wind toward the steady-state analytic solution (marked u_∞), when the slope is steep. With the gentler slope of 0.1°, which corresponds to the VL site slopes (Fig. 1b), the growth is much slower, but a deeper mass of air is involved. In Fig. 1c, the slope angle is kept at 0.1°, but the vertical diffusivity coefficients for momentum and heat (K_m, K_h) are calculated using the wind-shear- and stability-dependent model scheme described in section 2. (The resulting K_h at 12 h is also shown in Fig. 1c). The more realistic diffusion results in stronger winds near the surface and weaker winds aloft relative to the constant K case of Fig. 1b. Thus, a well-mixed upslope wind layer is formed over the warm Martian surface in Fig. 1c. As on Earth, if the slope is gentle, the upslope winds do not have time to grow into large values during daylight hours.

If the Coriolis force is now added to the Prandtl equations, the evolving flow will tend to turn to the right in the northern hemisphere of Mars with a period of 0.5 sol/sinϕ. This is demonstrated in Fig. 2 where the surface wind (1.6 m) hodographs are plotted for latitudes 10°, 30°, 50°, and 70°N for 0.1° slope using the Prandtl equations with the Coriolis force and the realistic diffusion of Fig. 1c. The initial (early morning) wind is set here to have a weak downslope component. The turning of the upslope wind is clear, with a 180° phase turn at 30°N in 12 h, as expected. The 50°N case is in fact not far from what was observed at daytime on VL-2 (cf. Fig. 5). A similar turning is expected also for the nighttime downslope wind. Here one cannot neglect radiative cooling on Mars, however, and it is best to consult the full model and observations.

4. The Martian slope winds: VL-2 observations and simulations

The VL-2 observations indicated rather weak ambient flow in summer, so it is perhaps instructive to start from that site, which is an east-increasing slope of 0.1° at 48°N, 225°W. The sol 2 afternoon (1400 LLT) model fields θ, u, v, w, for the VL-2 site summer conditions are shown in Fig. 3. Here the basic wind is zero so that the induced flow is entirely due to the slope effect. The time of the year is "22 July" (L_s = 115°; solar radiation is 530 W m^{-2} and solar declination angle 22°), and the afternoon ground is warm, T_g = 260 K. The PBL is seen to be well mixed up to 3.5 km, with westerly upslope wind ($u > 0$) over the slope in a 2-km deep layer (u_{max} = 0.95 m s^{-1}) and return flow aloft. Rising motion ($w > 0$) is concentrated near the top of the slope. The northward v values are positive over the whole slope area. This somewhat unexpected southerly wind component near the ground is in fact a remnant of the strong drainage flow from the previous night, as will be explained later.

Our 1400 LLT upslope wind values and the depth of the mixed layer are smaller than in Ye et al. (1990). This is caused (on top of model differences) by their higher terrain slope angles (0.23° and 0.57° vs 0.1°) and lower latitude (23° vs 48°N) and by their smaller soil heat capacity, leading to higher daytime surface temperatures. [For small terrain slope angles (<1°), the angle effect is nearly linear, as seen in Prandtl solutions and in Ye et al.'s results.] Our 2D model result is, however, in good agreement with the Prandtl solution (Fig. 1b,c; Fig. 2), in which the upslope wind was about 1 m s^{-1} 6–8 h after the heating was switched on. One could perhaps criticize Ye et al. (1990) in that

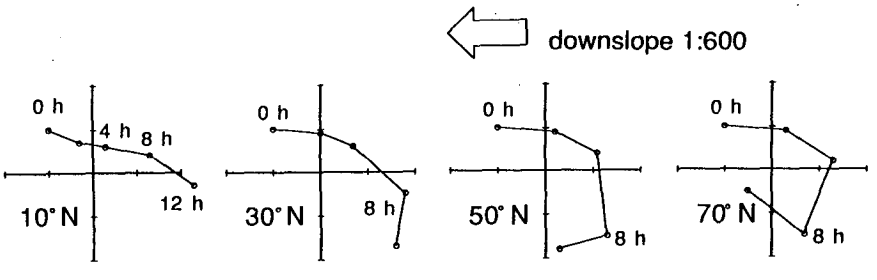

FIG. 2. As in Fig. 1c but for the 1.6-m wind hodograph at different latitudes, starting from $(u, v) = (-1, 1)$ m s^{-1} with the Coriolis force included. Unit in the u, v axes is 1 m s^{-1}.

they evidently started their simulation in the morning from rest, while in reality (and in our results) there is a strong drainage flow at sunrise, against which the developing upslope flow must work.

Figure 4 shows the model fields θ, u, v, w from the VL-2 case without basic flow but now in the morning, 0600 LLT, sol 2. The surface is cold (T_g = 185 K), and the PBL is very stable with a strong surface inversion below 1.5 km. There is easterly downhill drainage flow near the surface, which is 3.3 m s^{-1} near the surface. The downward motion is also seen in the w component just above the slope, in addition to the usual mass-conserving up–down circulation. The v field is here quite strong: 7.1 m s^{-1} at midslope at 100-m height. This southerly flow along the slope is triggered by the Coriolis force acting on the easterly component, and it accumulates during the night. It then tends to remain through the morning, as the developing upslope wind and the related opposite v is much weaker than the katabatic flow was and vertical mixing just redistributes and damps any existing v. The creation of this katabatic transverse jet near the surface thus depends on latitude, as will be discussed later. Unfortunately, its verification must await for the presently nonexistant wind observations in the nighttime Martian PBL; but if it is true, it could be significant, for example, for the movement of the planned MARS-94/96 mission observation balloons, which would heat up in the sunshine, rise every morning, travel with the winds, and land in the sunset. A somewhat analogous "transverse

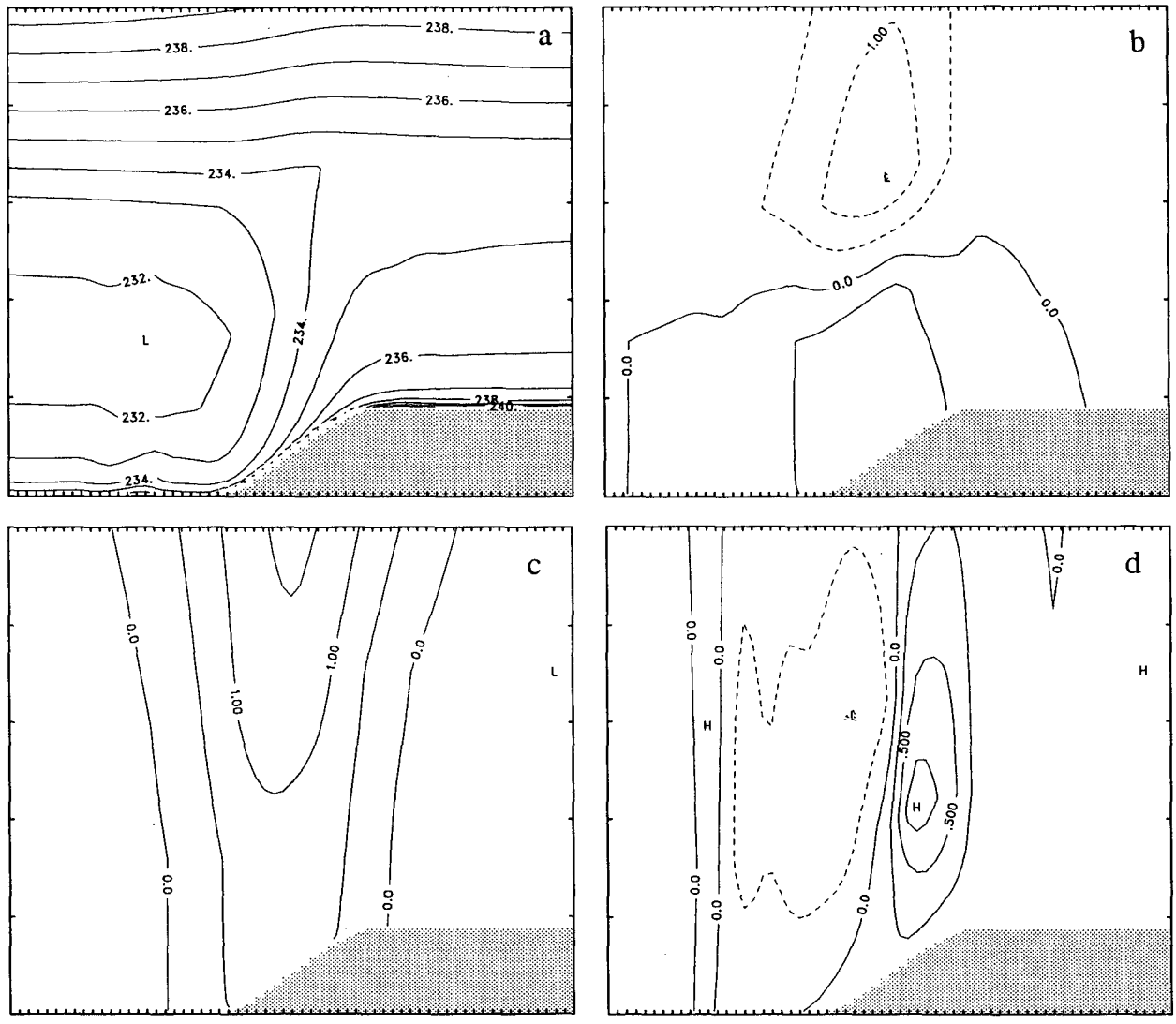

FIG. 3. "*Viking* Lander 2" case two-dimensional model results at 14 LLT. No basic wind. Vertical extent is 5 km; the east-growing 0.1° slope is 600 km long. Negative values are dashed. (a) Potential temperature θ, contour interval 1 K; (b) zonal-wind component u, contour interval 0.5 m s^{-1}; (c) meridional wind component v, contour interval 0.5 m s^{-1}; (d) vertical wind component w, contour interval 0.25 cm s^{-1}.

low-level jet" Coriolis effect on the sea breeze during offshore winds on Earth was simulated and discussed in Savijärvi and Alestalo (1988) and observed, for example, by Hsu (1979) off the Florida coast.

Both the upslope and downslope flow speeds are rather insensitive to the slope length. If the slope length is doubled in our simulations, the u, v patterns are just elongated along the slope, and the downslope maximum speed increases only 7%. This is in accordance with Mahrt's (1982) scaling arguments for drainage flows; the VL-2 case would fall on his "equilibrium class" where the flow speed does not depend on the distance traveled downslope.

Figure 5a shows the lowest-level (1.6 m) diurnal wind hodograph at midslope from the VL-2 case simulation without background flow. The averaged midsummer diurnal wind observations of VL-2 are also marked in the figure, taken from Leovy (1982, Fig. 11). One can see the upslope wind during daytime and downslope flow during the night in both sets, with the Coriolis force turning the wind clockwise, much as was seen in Fig. 2. The main difference between the observed and the simulated hodographs in Fig. 5a is that the simulated hodograph is shifted upward. This might indicate the existence of a weak prevailing large-scale northerly flow in the VL-2 site. As the GCM simulations of Pollack et al. (1981) suggest weak zonal mean northerlies for 48°N in summer in the lower Martian atmosphere, we added a 2 m s^{-1} northerly large-scale wind to the VL-2 simulation. This gives the hodograph in Fig. 5b. It is now quite close to what is observed. The largest differences occur at around sunset when the rapid and possibly stepwise collapse of the daytime well-mixed boundary layer (cf. Fig. 9) is hard to simulate by any

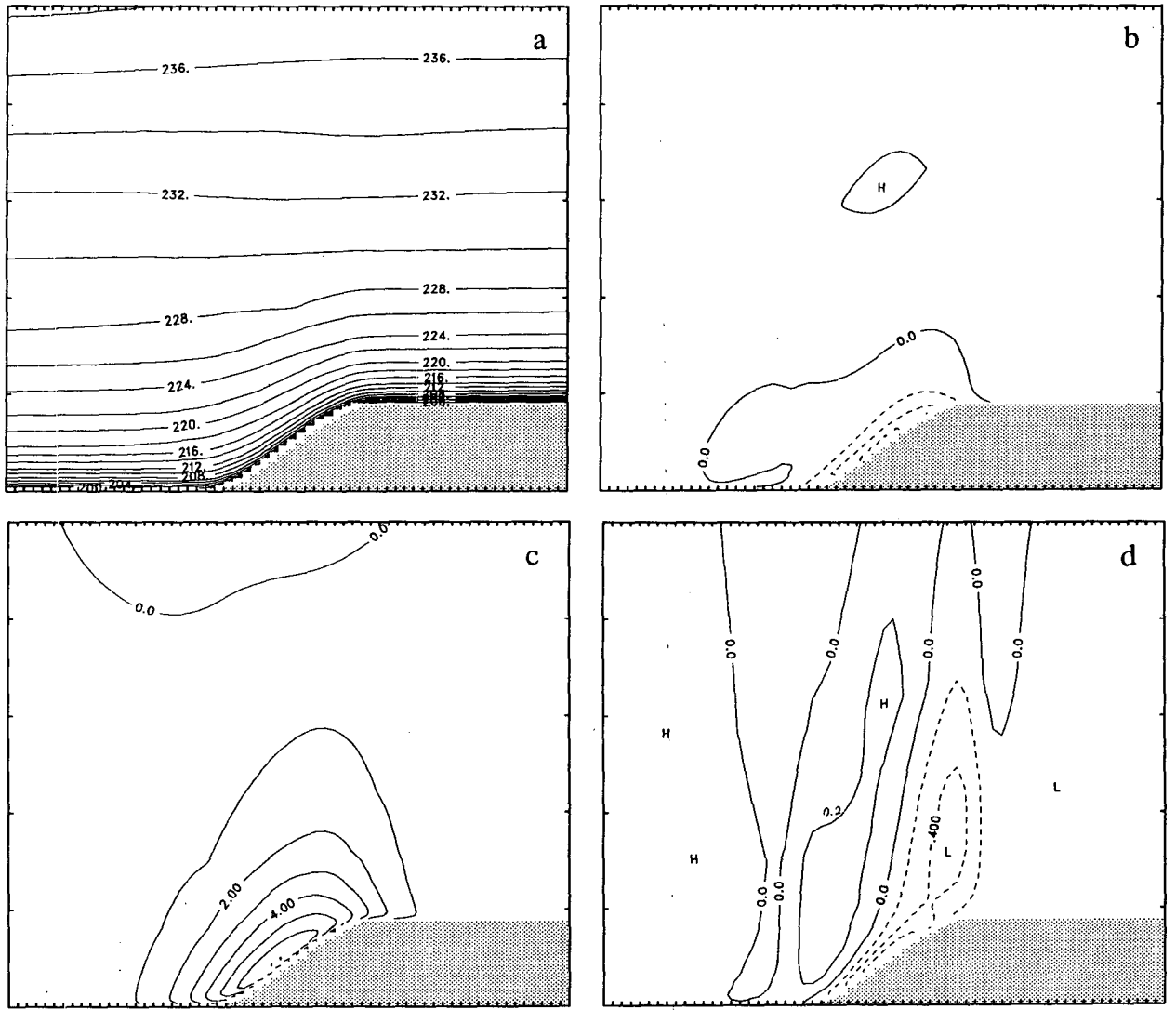

FIG. 4. As in Fig. 3 but for 0600 LLT. Contour intervals are 2 K, 1 m s^{-1}, 1 m s^{-1}, and 0.2 cm s^{-1}, respectively.

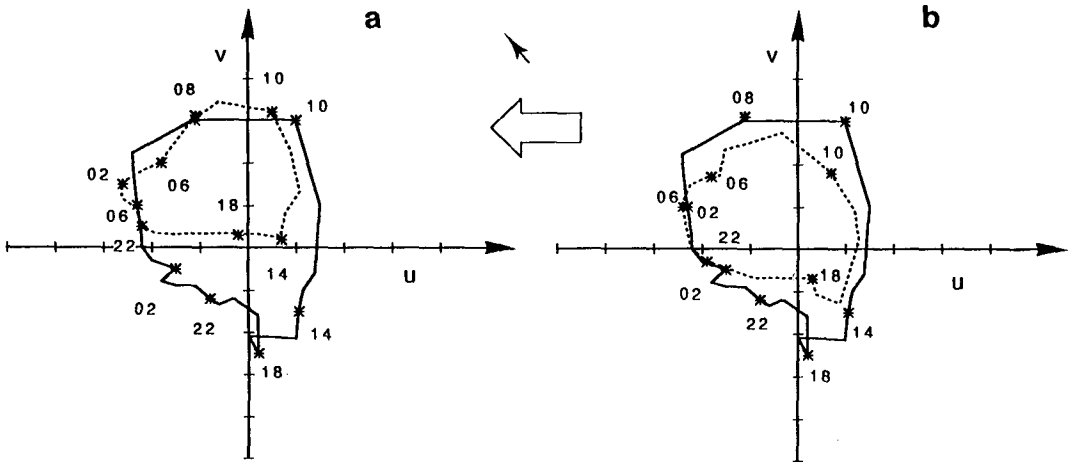

FIG. 5. Midsummer observed mean diurnal wind hodograph of VL-2 (solid, from Leovy 1982), and the 2D model 1.6-m hodograph (dashed). Black arrow points down the local slope (Leovy 1982) and white arrow down the large-scale 0.1° slope used in the model (Pollack et al. 1981 topography). Unit in the u, v axes is 1 m s^{-1}. (a) No basic wind; (b) 2 m s^{-1} northerly geostrophic wind in the model.

continuous turbulence scheme [cf. Savijärvi (1991a) for discussion of the Great Plains case]. Discontinuous collapse might lead to the irregular recurrent wandering of the observed VL-2 wind cycle near sunset. For the rest of the day, it seems that the quite regular diurnal wind cycle in the VL-2 summertime data is mainly due to the local slope wind variation on top of a fairly constant weak large-scale northerly flow. The slope winds do not interact strongly with the ambient flow but just superpose on it in Fig. 5.

Returning to the effect of latitude on the "transverse katabatic jet," Table 2 lists the extreme values of u and v and the maximum wind speed and direction over the westerly slope at 0600 LLT in the VL-2 case without basic flow at 48°N (from Fig. 4) and at 0°, 10°, 30°, and 70°N. Everything else, except latitude, is the same in the simulations. The patterns of u and v are in all cases analogous to those in Fig. 4. It can be seen that (the absolute value of) the downhill wind component u decreases with increasing latitude, being around 7 m s^{-1} for $0 < \phi < 40$°N, while the transverse component v increases with latitude until 50°N. At around 30°N there is thus still considerable drainage flow, u = 7.1 m s^{-1}, while the Coriolis force is now strong enough to increase v to 5.7 m s^{-1} so that the total wind speed is more than 9 m s^{-1}. [The peak in the wind speed at around 30°N can also be found in the analytic Prandtl solutions for Earth when the Coriolis force and cyclic diffusion are included (Paegle and Rasch 1973).] At high latitudes, both wind components are reduced. The reasons are that the Coriolis force now turns the katabatic flow strongly to the right, and surface friction then retards the total wind. Also, the summer night is now very short (late July at 70°N is nearly in the Martian midnight sun region, just like the northern parts of Finland), so the slope does not cool as effectively during the short night as in the lower latitudes.

The effect of latitude is smaller on the upslope flow because of the strong daytime vertical mixing on Mars.

5. The Martian local winds: VL-1 results, basic flow, and the nocturnal jet

The observations during and after the entry of VL-1 on "30 June" (L_s = 99°; S = 508 W m^{-2}, declination: 25°) and Pollack et al. (1976, 1981) GCM results indicate southerly upper flow at the VL-1 site, which was a west-growing 0.1° slope at 22.5°N, 48°W. Accordingly, we set 10 m s^{-1} constant geostrophic wind from the south. The large-scale upper wind thus blows along the slope in our 2D simulation, as do the prevailing summertime southwesterlies over the Great Plains, which also happen to have a slope of 0.1° and roughness length of a few centimeters.

The simulated midslope and the observed VL-1 midsummer diurnal 1.6-m wind hodographs are shown in Fig. 6a. The counterclockwise sense of rotation and the midnight and midday wind phases and amplitudes are well captured by the model, but the winds during the morning and evening transition periods are less

TABLE 2. The 06 LLT maximum drainage wind values at 100-m height in different latitudes. Other parameters are as for the VL-2 no-basic-wind experiment.

	(°N)				
Latitude	0	10	30	48	70
u (m s^{-1})	−7.8	−7.4	−7.1	−3.3	−2.2
v (m s^{-1})	0	1.5	5.7	7.1	5.8
Speed (m s^{-1})	7.8	7.6	9.1	7.8	6.2
Direction (deg)	90	101	130	155	160

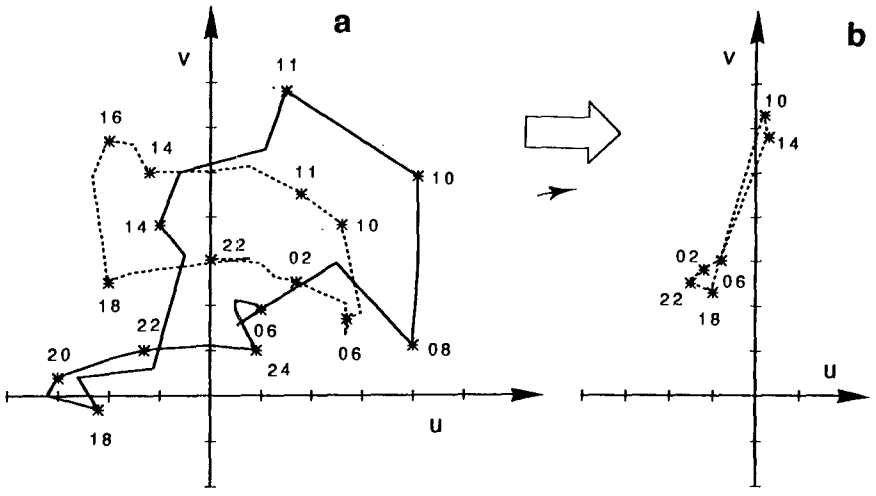

FIG. 6. (a) As in Fig. 5 but for VL-1, with 10 m s^{-1} southerly geostrophic wind in the model. (b) Model result without a slope but with the diurnal temperature variation and 10 m s^{-1} v_g.

accurate. It may be that the local slope angle and the actual large-scale winds were different from those in our idealized experiment. For instance, the diurnal thermal tides are probably stronger at the VL-1 latitude than at VL-2 (Zurek 1976) but they were not considered in the present experiments. Anyway, the slope wind mechanism is evident in Fig. 6a. For a demonstration of that, Fig. 6b shows the same 1.6-m wind hodograph but without any slope in the model. One can then see strong daytime and weak nighttime surface winds turned 10°–30° left from the geostrophic wind, as might be expected over a flat surface with strong diurnal temperature variation. It is this strong diurnal variation that helps to produce the counterclockwise rotation of the total surface wind in Fig. 6a, against the clockwise rotation of the Coriolis force action.

The afternoon (1400 LLT sol 2) u, v fields of the VL-1 experiment are shown in Figs. 7a,b. Since the surface temperatures are rather similar to those in the VL-2 case, and the slope angle is the same, the θ, u, and w fields are rather analogous to those in Fig. 3. The maximum upslope u wind is now 1.4 m s^{-1} versus 0.95 m s^{-1} in the VL-2 simulation. The v distribution (Fig. 7b) is dominated by the 10 m s^{-1} southerly upper flow, reduced by friction toward the surface. Smallest v values can be detected above the slope. This is an indication of the remnant of an early morning drainage katabatic transverse jet (here a northerly flow), now superposed on the southerly ambient wind.

The early morning (0600 LLT sol 2) VL-1 case u, v fields are shown in Figs. 7c,d. They can be compared with Fig. 4 of the VL-2 case, which was a pure slope wind at 48°N without basic flow. The downslope drainage flow u is stronger in the lower-latitude VL-1 case (5.1 m s^{-1} vs 3.3 m s^{-1}), while the slope-induced v component is a lot weaker in accordance with Table 2. Above the undisturbed level land areas, one can see cross-isobar Ekman flow in the shallow stable nighttime boundary layer (negative u values in Fig. 7c) driven by the southerly 10 m s^{-1} geostrophic wind.

There is a supergeostrophic wind (a nocturnal low-level jet) of 12 m s^{-1} at about 1-km altitude in Fig. 7d. This is studied more closely in Fig. 8, where the nighttime midslope wind hodograph of the VL-1 simulation is plotted at the 850-m level where the nocturnal low-level jet (NLLJ) is at its strongest in the model. The hodograph when the slope is removed from the model is also shown in Fig. 8. One can see some upslope flow during the afternoon in the slope 850-m hodograph, inertial oscillation during the night hours in both sets after turbulence is abruptly reduced in the evening (cf. Fig. 9), and some drainage flow in the morning in the slope hodograph. The amplitude of the oscillation is 2–3 m s^{-1}, which is also typical for the Great Plains. Most of the amplitude, and hence the Martian NLLJ, is caused by the inertial oscillation mechanism, suggested for Earth by Blackadar (1957). This can be seen in Fig. 8 by comparing the small difference between the slope and no-slope hodographs during and after midnight. The slope effect adds only 15%–20% to the NLLJ supergeostrophy. The same conclusion was drawn by Parish et al. (1988) from delicate flight observations during a Great Plains NLLJ episode and by Savijärvi (1991a) in a simulation of that episode and the average late spring conditions at the Great Plains. In this respect, our model predicts similar NLLJ behavior on Mars and Earth, in spite of the stronger forcing for the slope winds, that is, stronger diurnal surface temperature variation on Mars.

Quite considerable wind shears are thus expected at night and dawn in the lower part of the summertime Martian PBL. They should exist just about everywhere

whenever there is an ambient upper flow and over sloping regions every night, even when the prevailing flow is weak or nonexistent.

The model-produced vertical diffusion coefficients for heat (K_h) in the VL-1 simulation are shown in Fig. 9 as the function of time at several altitudes above the midslope point. One can see quick onset of convection in the morning, upward growth ("encroachment") of the mixed layer during the day, its collapse near sunset, and mechanical mixing during the night with maximum at the 200–300-m altitude. The model's diffusion coefficient for momentum K_m is about the same as K_h during the night and about 50% smaller than K_h during the day.

6. The Martian slope winds: A MARSNET site forecast

We will now apply our 2D model in a predictive mode to the three proposed meteorological observation system sites of the ESA MARSNET mission. The first of the three, a Lunae Planum site at 20°N, 63°W, is in fact quite close to the VL-1 site (800 km southwest of VL-1), with rather similar slope, surface, and prevailing flow characteristics. Therefore, our prediction here is simple: the summertime surface winds should be close to Fig. 6, and 850-m winds to Fig. 8. The other two sites are more interesting from our point of view. The Bosporos Planum site is at southern midlatitudes, −45°N, 70°W, on a downslope of 0.15° (1:400) to the

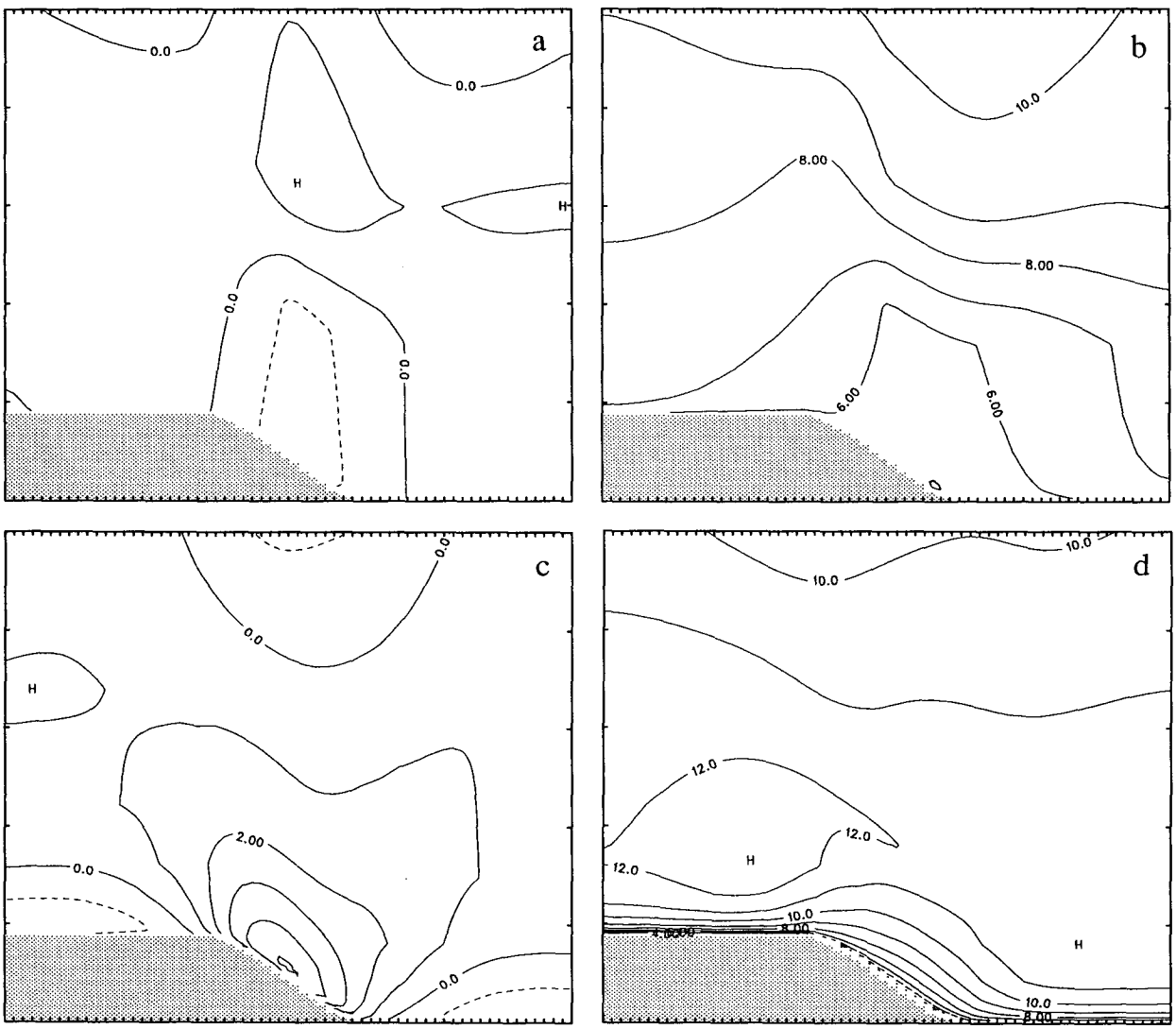

FIG. 7. Wind fields in the VL-1 simulation. Contour interval is 1 m s^{-1}, negative values are dashed. (a) u at 1400 LLT; (b) v at 1400 LLT; (c) u at 0600 LLT; and (d) v at 0600 LLT.

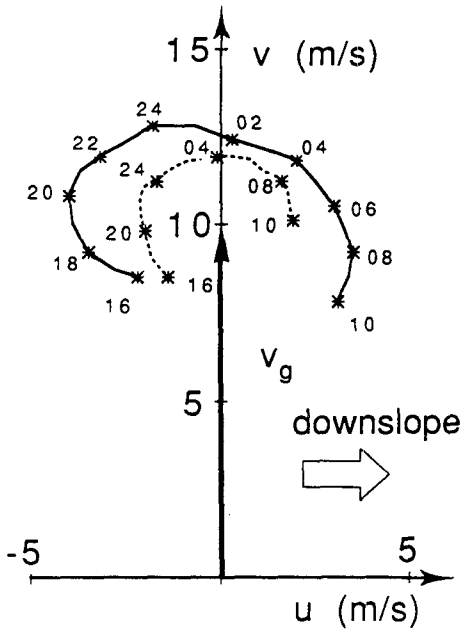

FIG. 8. The nighttime wind hodograph at 850-m height in the VL-1 simulation, with (solid) and without (dashed) the 0.1° slope in the model.

southeast, using again the large-scale topography of Pollack et al. (1981). The Arsia Mons site is nearer the equator in the southern hemisphere, −15°N, 120°W, on a steepish downslope of 0.27° (1:200) to the south-southwest, near the top of a high mountain.

We set $L_s = 310°$ ("30 January") to simulate southern summer conditions on Mars. Orbit calculations then give solar radiation S of 662 W m^{-2} and declination angle of −19.6° (note the high S during southern summer due to the ellipticity of Mars' orbit). The soil and dust characteristics were assumed to be the same as at VL-1 and VL-2 in summer. Initial air surface temperatures and pressures were modified to match the higher altitudes of the sites (Bosporos Planum is 2.5 km and Arsia Mons 6 km higher than VL-1); see Table 1. There is no basic wind in these experiments.

The predicted Bosporos Planum summertime diurnal temperature cycle was rather similar to those observed at VL-1 and VL-2, with slightly higher values (e.g., the 2-m daily maxima and minima of 249 K and 196 K vs 243 K and 189 K) due to the 30% higher solar radiation. The diurnal wind hodographs at 2-m and 85-m heights (Fig. 10) show upslope flow and a well-mixed structure during daytime and drainage flow with strong low-level vertical shear at night. The Coriolis force acts here to turn the flow to the left, and the counterclockwise southern midlatitude surface wind hodograph of Fig. 10 is like a mirror image of the northern midlatitude clockwise VL-2 hodograph of Fig. 5a. The wind speeds are enhanced, though, as the large-scale slope is now 50% steeper than at VL-2.

Figure 11 finally shows the expected 2-m and 85-m wind hodographs at Arsia Mons in summer with no prevailing flow. The proposed site is at a low latitude (−15°N), but high up on a mountain slope, and the

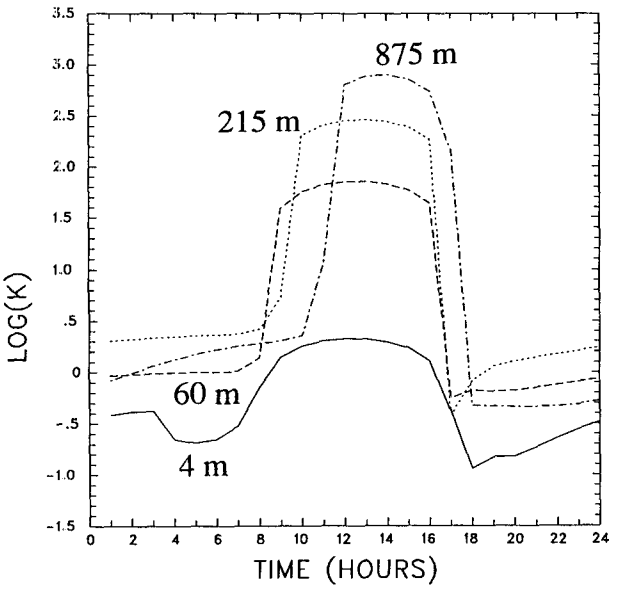

FIG. 9. Midslope vertical diffusion coefficient of heat ($\log_{10}K_h$) at several altitudes in the VL-1 simulation; K_h unit is m^2 s^{-1}.

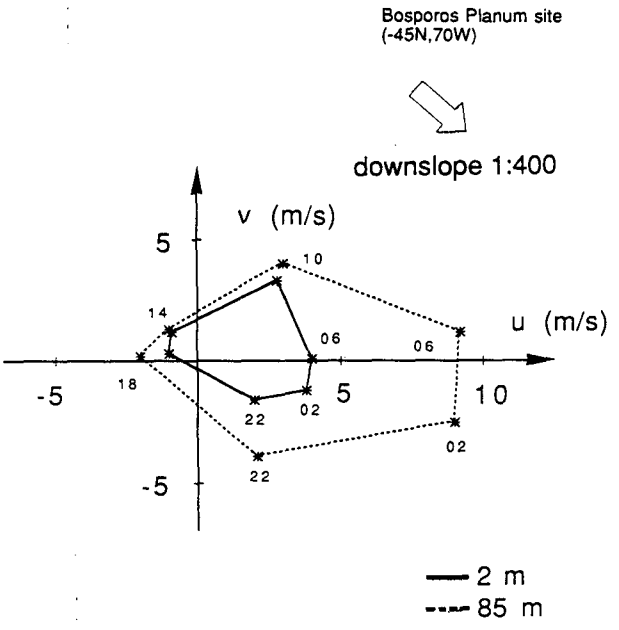

FIG. 10. The 2- and 85-m calm case predicted summertime diurnal wind hodographs for the ESA MARSNET Bosporos Planum site (−45°N, 70°W; slope 0.15°).

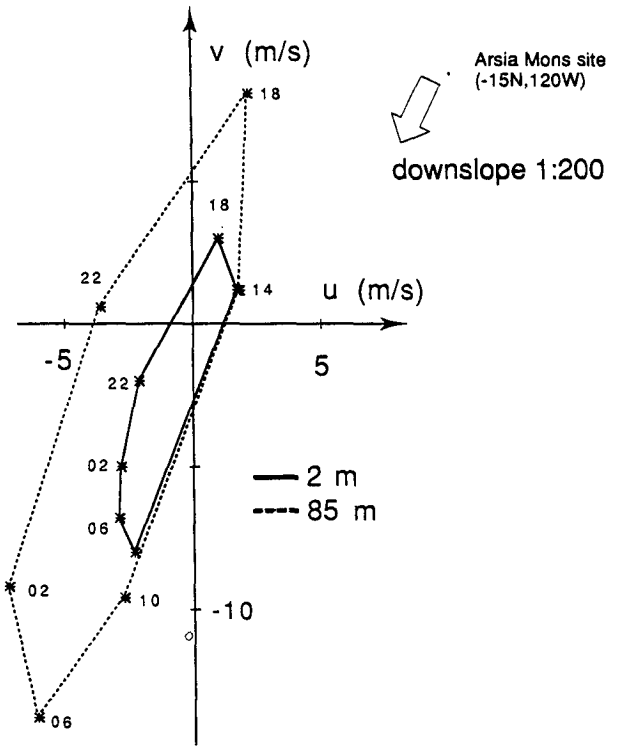

FIG. 11. As in Fig. 10 but for the Arsia Mons site (−15°N, 120°W; slope 0.26°).

simulated daily maxima and minima of 2-m temperatures were 245 K and 188 K. The combination of a steep slope and low latitude produces a considerable upslope–downslope wind structure, with a very quick transition between the well-mixed upslope flow in the unstable daytime PBL, and the strong drainage flow right down the cold nocturnal slope. At sunrise (0600 LLT), the 2-m wind speed is 7.5 m s^{-1}, and there is a downslope wind of 15–17 m s^{-1} to be expected at altitudes of 70–120 m. In contrast, the 1400 LLT upslope wind is only 2 m s^{-1}. Here the magnitude of the slope angle, latitude, and morning surface temperatures are not far from those in the basic experiment of Ye et al. (1990). Upslope winds of 4 m s^{-1}, similar to theirs, were reached at 1400 LLT when starting from rest at 0600 LLT; these were reduced to 2 m s^{-1} during the following sols in the simulation because of the preceding drainage winds.

If there is weak to moderate large-scale flow predicted, for example, by GCMs for these sites in summer, the "calm case" mesoscale wind roses of Figs. 10 and 11 may be superposed on the prevailing flow in the same way as in Figs. 5 and 6.

7. Conclusions

Slope winds and nocturnal low-level jets are probably ubiquitous in the Martian summer hemisphere where the diurnal surface temperature variation is large and the large-scale winds are weak. These Martian summertime PBL phenomena were simulated with a 2D mesoscale model, which was recently used for an analogous study on the Great Plains. The model's turbulence scheme was found to be reasonable in the simulation of the Great Plains typical late spring diurnal wind and temperature cycles (at least up to 420 m, based on mast data). Basically, the same Earth-validated turbulence and dynamics schemes were used, and the radiation and surface schemes were modified for Mars. Compared with the *Viking* lander data, the average summertime diurnal surface temperature and wind cycles and the VL entry temperature profiles were well simulated. This gives more credibility also to the other interesting results for Mars, listed below, for which there is no verification data at the moment.

During moderate large-scale upper flow, our model results indicate summertime Martian nocturnal low-level jets, which are rather similar to those on the Great Plains but are located perhaps slightly higher up (at 1 km). They are mainly caused by inertial oscillation after the rapid collapse of thermal turbulence at sunset and are thus expected to exist over flat as well as over sloping regions. The slope winds added 15%–20% to the low-level jet supergeostrophy of 3 m s^{-1} in VL-1 conditions, in the same manner as in the analogous Great Plains simulations.

During weak large-scale flow, our experiments predict a considerable and regular nocturnal drainage flow down the cold Martian nighttime slopes, with maximum winds at about 100-m height (17 m s^{-1} was obtained for a proposed ESA MARSNET mission observation site over the relatively steep slope of Arsia Mons). For a fixed slope angle and no basic flow, maximum drainage flow speeds are expected at latitudes 25°–35° (Table 2). In higher latitudes, this drainage flow, initially down the slope, is slowly turned by the Coriolis force during the Martian night. Thus, the high-latitude low-level wind is expected to be more or less along the slope in the summer dawn: a "geodynamic paradox" where the flow is at cross angles with its forcing.

The Martian daytime upslope flow evolves only slowly in our model (unless the slope is very steep), similar to the Great Plains simulations and Prandtl's slope wind theory. During daytime, the convective Martian PBL grows up to 4–5 km in the late afternoon. This keeps winds rather well-mixed vertically. Because of these two reasons, the Martian daytime anabatic upslope winds are not strong (1–4 m s^{-1}). They extend quite homogeneously up to 2–3 km in the afternoon. In contrast, the much stronger and shallower nocturnal katabatic downslope flows can produce formidable vertical shear near the surface.

Predictions for the local summertime diurnal wind and temperature cycles for two proposed MARSNET

mission sites are finally presented. We are looking forward to verifying them some day.

Acknowledgments. C. Fortelius, J. Kaurola, and H. Järvinen are acknowledged for their help in the text and figure editing.

REFERENCES

Alestalo, M., and H. Savijärvi, 1985: Mesoscale circulations in a hydrostatic model: Coastal convergence and orographic lifting. *Tellus,* **37A,** 156–162.

Alpert, P., A. Cohen, E. Doron, and J. Neumann, 1982: A model simulation of the summer circulation from the Eastern Mediterranean past Lake Kinneret in the Jordan valley. *Mon. Wea. Rev.,* **110,** 994–1006.

Blackadar, A. K., 1957: Boundary-layer wind maxima and their significance for the growth of nocturnal inversions. *Bull. Amer. Meteor. Soc.,* **38,** 283–290.

Blumsack, S. L., P. J. Gierasch, and W. R. Wessel, 1973: An analytical and numerical study of the Martian planetary boundary layer over slopes. *J. Atmos. Sci.,* **30,** 66–82.

Chicarro, A. F., M. Coradini, M. Fulchignoni, I. Liede, P. Lognonne, J. M. Knudsen, G. E. N. Scoon, and H. Wänke, 1991: MARSNET Assessment Study Rep., ESA Publication SCI(91)6, 121 pp. [Available from ESA HQ(D/SCI), 8-10 rue Mario Nikis, 75738 Paris Cedex 15, France.]

Dickinson, R. E., 1988: The force-restore model for surface temperatures and its generalizations. *J. Climate,* **1,** 1086–1097.

Haberle, R. M., 1986: The climate of Mars. *Sci. Amer.,* **254**(5), 42–57.

Hess, S. L., R. M. Henry, C. B. Leovy, J. A. Ryan, and J. E. Tillman, 1977: Meteorological results from the surface of Mars: Viking 1 and 2. *J. Geophys. Res.,* **82,** 4559–4574.

Hsu, S. A., 1979: Mesoscale nocturnal jetlike winds within the planetary boundary layer over a flat, open coast. *Bound.-Layer Meteor.,* **17,** 485–494.

Leovy, C. B., 1982: Martian meteorological variability. *Adv. Space Res.,* **2,** 19–44.

Louis, J.-F., 1979: A parametric model of vertical eddy fluxes in the atmosphere. *Bound.-Layer Meteor.,* **17,** 187–202.

Mahrt, L., 1982: Momentum balance of gravity flows. *J. Atmos. Sci.,* **39,** 2701–2711.

Neumann, J., and H. Savijärvi, 1986: The sea breeze on a steep coast. *Contrib. Atmos. Phys.,* **59,** 375–389.

Paegle, J., and G. Rasch, 1973: Three-dimensional characteristics of diurnally varying boundary-layer flows. *Mon. Wea. Rev.,* **101,** 746–756.

Parish, T. R., A. R. Rodi, and R. D. Clark, 1988: A case study of the summertime Great Plains low-level jet. *Mon. Wea. Rev.,* **116,** 94–105.

Pollack, J. B., 1982: Properties of dust in the Martian atmosphere and its effect on temperature structure. *Adv. Space Res.,* **2,** 45–56.

——, 1991: Present and past climates of the terrestrial planets. *Icarus,* **91,** 173–198.

——, C. B. Leovy, Y. Mintz, and W. Van Kamp, 1976: Winds on Mars during the Viking season: Predictions based on a general circulation model with topography. *Geophys. Res. Lett.,* **3,** 479–482.

——, ——, P. W. Greiman, and Y. Mintz, 1981: A Martian general circulation experiment with large topography. *J. Atmos. Sci.,* **38,** 3–29.

Savijärvi, H., 1985: The sea breeze and urban heat island in a numerical model. *Geophysica,* **21,** 115–126.

——, 1991a: The United States Great Plains diurnal ABL variation and the nocturnal low-level jet. *Mon. Wea. Rev.,* **119,** 833–840.

——, 1991b: Radiative fluxes on a dustfree Mars. *Contrib. Atmos. Phys.,* **64,** 103–112.

——, 1991c: A model study of the PBL structure on Mars and the Earth. *Contrib. Atmos. Phys.,* **64,** 219–229.

——, and M. Alestalo, 1988: The sea breeze over a lake or gulf as the function of the prevailing flow. *Contrib. Atmos. Phys.,* **61,** 98–104.

Stull, R. B., 1988: *An Introduction to Boundary Layer Meteorology.* Kluwer Academic, 666 pp.

Sutton, J. L., C. B. Leovy, and J. E. Tillman, 1978: Diurnal variations of the Martian surface layer meteorological parameters during the first 45 sols at two Viking lander sites. *J. Atmos. Sci.,* **35,** 2346–2355.

Vihma, T., and H. Savijärvi, 1991: On the effective roughness length over heterogeneous terrain. *Quart. J. Roy. Meteor. Soc.,* **117,** 399–408.

Ye, Z. J., M. Segal, and R. A. Pielke, 1990: A comparative study of daytime thermally induced upslope flow on Mars and Earth. *J. Atmos. Sci.,* **47,** 612–628.

Zurek, R. W., 1976: Diurnal tide in the Martian atmosphere. *J. Atmos. Sci.,* **33,** 321–337.